$(Ti,Sn)O_2$ Mixed Oxides Nanoparticles Obtained by the Sol−Gel Route

Marcela M. Oliveira, Danielle C. Schnitzler, and Aldo J. G. Zarbin*

Departamento de Química, Universidade Federal do Paraná (UFPR), CP 19081, CEP 81531-990, Curitiba, Paraná, Brazil

Received October 21, 2002. Revised Manuscript Received February 19, 2003

This paper focuses on the preparation and characterization of a titanium−tin mixed oxide $(Ti,Sn)O_2$ with anatase structure. The preparation method is based on a sol−gel technique using titanium tetra-isopropoxide and tin tetrachloride as precursors. The obtained TiO_2 and titanium−tin mixed oxide xerogels and their heat-treated products were characterized by thermal analysis, X-ray diffractometry, Raman spectroscopy, and X-ray absorption spectroscopy. The results indicate that the $(Ti,Sn)O_2$ was obtained in the nanometer scale and the crystallite size was smaller than the pure TiO_2 obtained by a similar route. The mixed oxide was obtained as a solid solution. Compared to the bulk TiO_2, the Raman spectra of both TiO_2 and $(Ti,Sn)O_2$ xerogels present an excessive E_g peak broadening, which was attributed to the presence of surface low-coordinated titanium atoms. The occurrence of these species was confirmed by XANES and EXAFS spectra of both pure TiO_2 and $(Ti,Sn)O_2$ xerogels.

Introduction

Titanium oxide produced by the sol−gel route is an important material of great interest for applications in the fields of photocatalysis, optics, photovoltaics, and so forth.[1−3] The sol−gel process involves the low-temperature synthesis of an inorganic network by a chemical reaction in solution, generally the hydrolysis and subsequent peptization of metallic alkoxides.[4,5] Many variables can influence the quality of the final product, for example, the choice of the solvent, use of acid or base catalysis, and use of stabilizing agents.[4−7] One of the many advantages of the sol−gel process is the possibility of forming well-controlled mixed oxides, by a judicious choice of the used precursors.[4,8−10]

Mixed oxides have received great attention in recent years. Material research on mixed oxides has been performed for practical application in optical and electric devices,[11,12] gas sensors,[13−15] catalytic and photocatalytic materials,[16] and so forth. Recently, Zakrzewska[13] showed that mixed oxide systems can be classified into three categories: (i) the category where the formation of distinct chemical compounds, like the $ZnO−SnO_2$ systems in which $ZnSnO_3$ and Zn_2SnO_4 are formed, occurs; (ii) the category where the formation of solid solutions, like $TiO_2−SnO_2$, occurs; and (iii) systems that form neither new compounds nor solid solutions, like $TiO_2−WO_3$.

There are several studies concerning the mixed-oxide $TiO_2−SnO_2$ systems.[12,13,15] It is well-known that TiO_2 and SnO_2 form rutile-type solid solutions over the entire range of compositions at high temperatures.[12,13] Rutile solid solutions from these oxides ($Ti_xSn_{1-x}O_2$) have been prepared as powder and thin films using several materials and experimental methods, such as sol−gel, coprecipitation, solid-state reactions, and r.f. sputtering.[13] However, to our knowledge there are no reports on the anatase $TiO_2−SnO_2$ solid solution in the literature. The anatase structure of TiO_2 shows substantially higher photoactivity than the rutile one.[17−19] The use of bicomponent TiO_2/SnO_2 as a photocatalyst improves the photoactivity due to an increase of charge separation of photogenerated electrons and holes within the system, suppressing recombination.[20−22] By this way, the $TiO_2−SnO_2$ solid solution with the anatase structure

* To whom correspondence should be addressed. E-mail: aldo@quimica.ufpr.br.

(1) Pichot, F.; Pitts, J. R.; Gregg, B. A. *Langmuir* **2000**, *16*, 5626.
(2) Nam, H. J.; Itoh, K.; Murabayashi, M. *Electrochemistry* **2002**, *70*, 429.
(3) Horikoshi, S.; Watanabe, N.; Hidaka, H.; Serpone, N. *New J. Chem.* **2002**, *26*, 1161.
(4) Sakka, S.; Kamiya, K. *J. Non-Cryst. Solids* **1980**, *42*, 403.
(5) Hench, L. L.; West, J. K. *Chem. Rev.* **1990**, *90*, 33.
(6) Yoldas, B. E. *J. Mater. Sci.* **1986**, *21*, 1087.
(7) Bischoff, B. L.; Anderson, M. A. *Chem. Mater.* **1995**, *7*, 1772.
(8) Livage, J.; Sanchez, C.; Barbonneau, F. *Chemistry of Advanced Materials: An Overview*; Interrante, L. V., Hampden-Smith, M. J., Eds.; Wiley-VCH: New York, 1998.
(9) Armelao, L.; Fabrizio, M.; Gross, S.; Martucci, A.; Tondello, E. *J. Mater. Chem.* **2000**, *10*, 1147.
(10) Veith, M. *J. Chem. Soc., Dalton Trans.* **2002**, *12*, 2405.
(11) Purans, J.; Azens, A.; Granqvist, C. G. *Electrochim. Acta* **2001**, *46*, 2055.
(12) Komornicki, S.; Radecka, M.; Rekas, M. *J. Mater. Sci-Mater. Electron.* **2001**, *12*, 11.
(13) Zakrewska, K. *Thin Solid Films* **2001**, *391*, 229.
(14) Dusastre, V.; Williams, D. E. *J. Mater. Chem.* **1999**, *9*, 445.
(15) Radecka, M.; Zakrzewska, K.; Rekas, M. *Sensors Actuators B* **1998**, *47*, 194.
(16) Dagan, G.; Sampath, S.; Lev, O. *Chem. Mater.* **1995**, *7*, 446.
(17) Kominami, H.; Matsuura, T.; Iwai, K.; OTAN, B.; Nishimoto, S.; Kera, Y.; *Chem. Lett.* **1995**, *11*, 693.
(18) Di Paola, A.; Marci, G.; Palmisano, L.; Schiavello, M.; Uosaki, K.; Ikeda, S.; Ohtani, B. *J. Phys. Chem. B* **2002**, *106*, 637.
(19) Pecchi, G.; Reyes, P.; Sanhueza, P.; Villaseñor, J. *Chemosphere* **2001**, *43*, 141.
(20) Tada, H.; Hattori, A.; Tokihisa, Y.; Imai, K.; Tohge, N.; Ito, S. *J. Phys. Chem. B* **2000**, *104*, 4585.
(21) Kawahara, T.; Konishi, Y.; Tada, H.; Tohge, N.; Ito, S. *Langmuir* **2001**, *17*, 7442.

10.1021/cm0210344 CCC: $25.00
Published on Web 04/05/2003

could be a material with an excellent potential to photocatalysis.

In this paper we report the preparation of an anatase-type TiO_2-SnO_2 solid solution using the sol−gel process. The samples have been characterized by X-ray diffractometry (XRD), infrared (IR) and Raman spectroscopy, thermogravimetric analysis (TGA), differential scanning calorimetry (DSC), X-ray near-edge structure (XANES), and extended X-ray absorption fine structure (EXAFS).

Experimental Section

Titanium oxide was prepared based on the method described by Bischoff and Anderson:[7] 10 mL of titanium tetra-isopropoxide (TTIP, Strean product), used without further purification, was diluted in 30 mL of 2-propanol (Carlo Erba). This mixture was added in 50 mL of Milli-Q filtered H_2O into which 0.5 mL of concentrated nitric acid (Merck) was added previously. Precipitation occurred immediately. The precipitate was then peptized with the available HNO_3 at 60 °C for 8 h in a reflux system. After this the reaction was stirred for 8 h at room temperature, followed by evaporation of 2-propanol and water at 55 °C for a week. The 55 °C drying gel was stored in a desiccator for further characterization. This sample will be referred to here as TiO_2−xerogel.

The sample TiO_2-SnO_2 was obtained with approximately 10% in weight of tin, as follows: in a glovebox 0.5 mL of $SnCl_4$ (Riedel) was previously stirred with 12.5 mL of 2-propanol for 10 min, followed by the addition of 12.5 mL of TTIP. This mixture was stirred for 10 min more and subsequently was slowly added to 75 mL of Milli-Q H_2O into which 0.52 mL of concentrated nitric acid was added previously. The sequence of peptization, drying, and storage of the samples was similar to the one described above. The sample obtained after the 55 °C drying step will be referred to here as $(Ti,Sn)O_2$−xerogel.

The heat treatment of the samples was carried out in an alumina crucible. Approximately 0.2 g of sample was added in a furnace at room temperature. The temperature was raised at 5 °C min^{-1} until the maximum requested (100−1000 °C) and maintained over a period of 2 h in ambient atmosphere. Then, the samples were cooled and stored in a desiccator.

XRD patterns were obtained in a Phillips difractometer, using Co Kα radiation with 40 kV and 20 mA, at a 0.2° scan rate (in 2θ). The room-temperature measurements were performed with the samples spread on a conventional glass sample holder. Powder silicon reflections were used for 2θ calibration. The identification of crystal structure was made using d spacings at 3.52 Å (101) for anatase, 3.25 Å (110) for rutile, and 2.90 Å (121) for brookite. The areas of the XRD peaks were evaluated by Gaussian decovolution using the Origin 5.0 program. The crystallite diameter was determinate employing peak-broadening analysis utilizing the Scherrer's equation.

The Raman spectra were obtained in a Renishaw Raman image spectrophotometer, coupled to an optical microscope that focuses the incident radiation down to an ≈1-μm spot. A He−Ne laser (emitting at 632.8 nm) was used, with incidence potency of 2 mW over the 2000−100-cm^{-1} region. The width of the E_g anatase band in each spectra was obtained after a Lorentzian deconvolution with the Origin 5.0 program.

TGA/DSC measurements were carried out simultaneously in Netzsch STA 409 equipment, in static air. Approximately 15 mg of each sample was analyzed between 20 and 1000 °C at 8 °C min^{-1}, using alumina crucibles.

The XAS experiments were performed on the XAS beam line of the National Synchrotron Light Laboratory (LNLS, Brazil).[23] EXAFS and XANES spectra were collected at the titanium K-edge (4965 eV) using a Si(111) monochromator calibrated at the K-edge of metallic titanium. XANES spectra were also collected at the tin L_3-edge (3929 eV) using the same monochromator. TiO_2 anatase, TiO_2 rutile, and SnO_2 cassiterite (rutile) were used as reference compounds. The experimental XANES spectra were collected with a resolution around 0.3 eV, were background-corrected using a Victoreen-fit in the 4866−4920-eV region, and were normalized in the range of 5000−5530 eV. This procedure was realized using the program WINXAS.[24] The peaks in the normalized XANES spectra were Gaussian-deconvoluted using the program Origin 5.0. The EXAFS spectra were normalized, analyzed, and fitted using the WINXAS code. To fit the EXAFS spectra, a crystalline anatase sample was used as reference. The values of nearest-neighbor atoms (N) and their distance (R) were obtained from the anatase crystallographic data. The Debye−Waller factors of reference anatase were assumed to be zero.

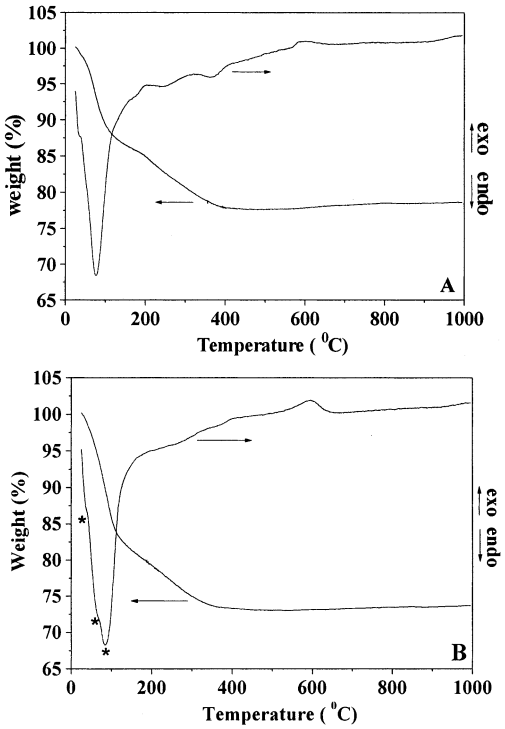

Figure 1. TGA and DSC curves: (A) TiO_2 xerogel; (B) $(Ti,Sn)O_2$ xerogel.

Results and Discussion

The thermal behavior of TiO_2 and $(Ti,Sn)O_2$ xerogels was investigated by thermogravimetry (TG) and differential scanning calorimetry (DSC), and the results are shown in Figure 1. The DSC curve of TiO_2 xerogel (Figure 1A) exhibits two endothermic events at 36 and 79 °C corresponding to 14.5% weight loss until 186 °C, which are associated with the elimination of adsorbed water and alcohol. The 7.7% weight loss observed in the range 200−400 °C is accompanied by two broad and weak endothermic features and is attributed to the dehydroxylation process of surface-attached H_2O and OH groups.[25] At temperatures higher than 400 °C no significant weight loss is observed in the TG curve. The exothermic peak centered at 605 °C is attributed to the anatase−rutile transition,[26] as confirmed by XRD data

(22) Cao, Y.; Zhang, X.; Yang, W.; Du, H.; Bai, Y.; Li, T.; Yao, J. *Chem. Mater.* **2000**, *12*, 3445.

(23) Tolentino, H.; Cezar, J. C.; Cruz, D. Z.; Campagnon-Cailhol, V.; Tamura, E.; Alves, M. C. M. *J. Synchrotron Radiat.* **1998**, *5*, 521.

(24) Ressler, T. *J. Phys. IV* **1997**, *7*, 269.

(25) Alemany, L. J.; Bañares, M. A.; Pardo, E.; Martín-Jiménez, F.; Blasco, J. M. *Mater. Charact.* **2000**, *44*, 271.

(26) Dassler, A.; Feltz, A.; Jung, J.; Ludwig, W.; Kaiserberger, E. *J. Therm. Anal.* **1998**, *33*, 803.

Table 1. XRD and Raman Data of Samples

sample	crystallite size[a] (nm)	position E_g band (cm^{-1})	fwhm E_g band (cm^{-1})
TiO_2 anatase[b]		145	20.5
TiO_2 xerogel	4.8	156	38.4
TiO_2 xerogel, 200 °C	6.6	151	32.5
TiO_2 xerogel, 400 °C	8.9	149	23.8
TiO_2 xerogel, 600 °C		146	22.9
(Ti,Sn)O_2 xerogel	3.2	157	41.2
(Ti,Sn)O_2 xerogel, 200 °C	5.1	154	37.0
(Ti,Sn)O_2 xerogel, 400 °C	6.5	149	30.2
(Ti,Sn)O_2 xerogel, 600 °C		147	27.0

[a] From Scherrer's equation; [b] Commercial reference sample

(discussed latter). The TG/DSC profile of the (Ti,Sn)-O_2-xerogel (Figure 1-B) is essentially similar to that observed for the TiO_2 xerogel, except in the following: (i) the DSC profile in the region associated with the elimination of water and alcohol (~25−150 °C) presents three endothermic peaks at 37, 67, and 85 °C (marked with asterisks in Figure 1B), which can be an indicative that the (Ti,Sn)O_2 xerogel surface properties are different from those of the TiO_2 xerogel (which shows only two endothermic events in this region); (ii) the total weight loss observed in the TGA curve (26.7%) is higher than that in the TiO_2 xerogel (22.2%).

The phase composition in both TiO_2 and (Ti,Sn)O_2 was established by powder X-ray diffractometry (XRD) performed on xerogels and heat-treated (100−1000 °C) powders. XRD data for TiO_2 (not shown) indicated that the oxide was formed in the majority in the anatase structure with a minor brookite component, as previously reported by Bischoff and Anderson.[7] The anatase structure of TiO_2 remains stable until 400 °C. The XRD pattern of TiO_2 xerogel heated at 600 °C shows peaks characteristic of the rutile phase, with some anatase peaks remaining, indicating that the phase transition anatase from rutile occurs in the temperature close to 600 °C, consistent with the exothermic peak at 605 °C observed in the DSC curve. At temperatures higher than 600 °C only the rutile phase was observed. We observed broad peaks on the TiO_2 xerogel XRD pattern that indicates short crystallite diameter of the former oxide, which was estimated by Scherrer's equation as 4.8 nm. Results obtained by Scherrer's equation suggest that the crystallite size increases as the temperature increases. The XRD patterns of the material heat-treated at temperatures higher than 400 °C show sharper diffraction profiles corresponding to crystallite growth, as confirmed by the average crystallite size determined by Scherrer's formula. The data of crystallite size of samples are summarized in Table 1.

The XRD results of (Ti,Sn)O_2 xerogel, presented in Figure 2, indicate that no significant structural variation occurs when compared with those of the pure TiO_2. As can be seen, the phases obtained by thermal treatment of the (Ti,Sn)O_2 are very similar to those obtained for pure TiO_2 (discussed before). The absence of a SnO_2-related secondary phase was observed in the xerogel and after heat treatment in the range of 100−1000 °C, which suggests the formation of a solid solution. Despite the similar results observed for the XRD of TiO_2 and (Ti,-Sn)O_2 xerogel, it was observed through Scherrer's equation that the mixed-oxide material presents smaller particles than the pure TiO_2. For the (Ti,Sn)O_2 xerogel

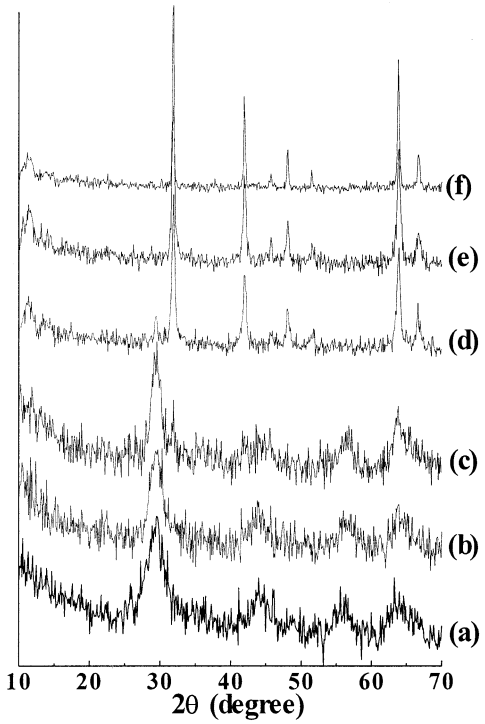

Figure 2. X-ray diffraction profile of (Ti,Sn)O_2 xerogel (a) and (Ti,Sn)O_2 xerogel heat-treated at 200 °C (b), 400 °C (c), 600 °C (d), 800 °C (e), and 1000 °C (f).

a crystallite size of 3.2 nm was observed, whereas it goes to 5.1 at 200 °C and 6.5 at 400 °C (Table 1).

The phase evolution of the oxides obtained in this work was also investigated by Raman spectroscopy. In Figure 3 we show the Raman spectra of TiO_2 (I) and (Ti,Sn)O_2 (II) xerogel powders after different heat-treatment temperatures. The commercial pure anatase and the pure SnO_2 spectra are also shown for comparison. The Raman spectrum of commercial TiO_2 exhibits a very intense band at 145 cm^{-1} (E_g band) and three other bands at 397, 518, and 639 cm^{-1} (B_{1g}, $A_{1g} + B_{1g}$, and E_g modes, respectively), all characteristics of the anatase form of TiO_2.[27−30] The Raman spectrum of TiO_2 xerogel shows all the anatase bands plus a series of bands at 246, 324, 365, and 632 cm^{-1} attributed to the brookite phase,[25,28] which confirms the occurrence of traces of brookite in the TiO_2 obtained in this work. Bands assigned to the rutile phase,[25,28,30] at 447 and 610 cm^{-1}, appeared in the spectrum when the sample was heated at 600 °C, showing a coexistence of anatase, brookite, and rutile phase in this temperature. At 800 and 1000 °C the spectra show only the rutile bands at 147, 235, 447, and 610 cm^{-1} .[25,28,30] These results are in agreement with both the XRD and DSC data.

The (Ti,Sn)O_2 xerogel spectrum shows no bands attributed to pure SnO_2, which corroborate the XRD conclusion that the mixed oxide was formed as a solid solution. As can be seen in Figure 3, the profiles of the

(27) Zeng, T.; Qiu, Y.; Chen, L.; Song, X. *Mater. Chem. Phys.* **1998**, *56*, 163.
(28) Music, S.; Gotic, M.; Ivanda, M.; Popovic, S.; Turkovic, A.; Trojko, R.; Sekulic, A.; Furic, K. *Mater. Sci. Eng. B* **1997**, *47*, 33.
(29) Falaras, P.; Goff, A. H−L.; Bernard, M. C.; Xagas, A. *Sol. Energy Mater. Sol. Cells* **2000**, *64*, 167.
(30) Gajovic, A. Stubicar, M.; Ivanda, M.; Furic, K. *J. Mol. Struct.* **2001**, *563−564*, 315.

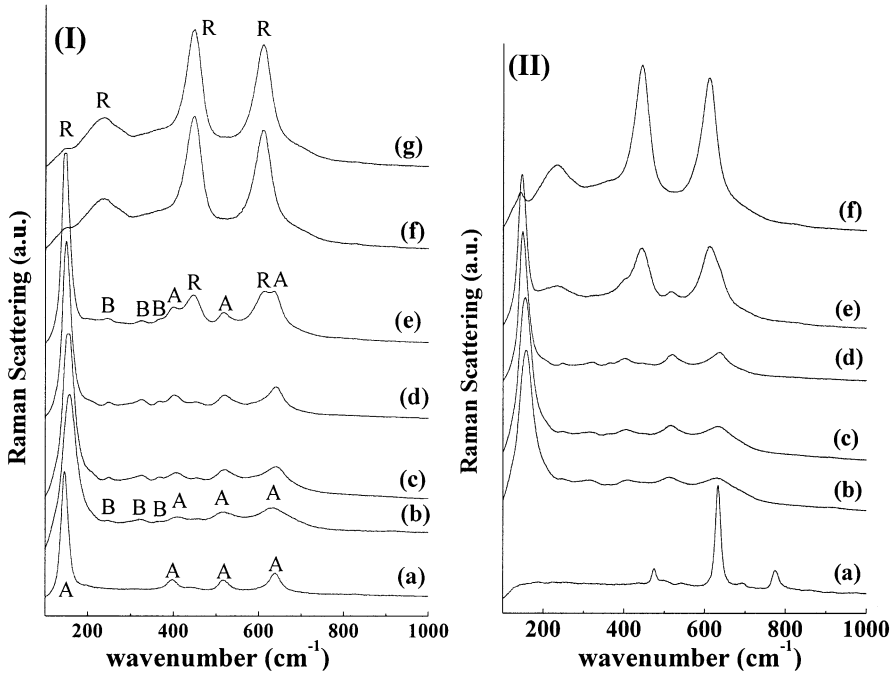

Figure 3. (I) Raman spectra of commercial anatase TiO_2 (a), TiO_2 xerogel (b), and TiO_2 xerogel heat-treated at 200 °C (c), 400 °C (d), 600 °C (e), 800 °C (f), and 1000 °C (g). (II) Raman spectra of commercial SnO_2 (a), $(Ti,Sn)O_2$ xerogel (b), and $(Ti,Sn)O_2$ xerogel heat-treated at 200 °C (c), 400 °C (d), 600 °C (e), and 1000 °C (f). A = anatase, B = brookite, and R = rutile.

$(Ti,Sn)O_2$ xerogel and heat-treated spectra are very similar to those of the pure TiO_2 discussed above.

It has been reported that Raman scattering can be used for an estimation of a TiO_2 crystallite size, by examining the TiO_2 E_g mode.[29,31−33] This band appears at ∼143 cm^{-1} in bulk anatase and shifts to higher wavenumbers (∼154 cm^{-1}) in nanocrystalline materials. The spectra presented in Figure 3 show the E_g band at 145 cm^{-1} for commercial TiO_2, at 156 cm^{-1} for TiO_2 xerogel, and at 157 cm^{-1} for $(Ti,Sn)O_2$ xerogel, confirming that the oxides are obtained with particles in the nanometric size. This band shifts to 146 and 147 cm^{-1} for the 600 °C thermal-treated TiO_2 and $(Ti,Sn)O_2$, respectively, as a consequence of the crystallite growth observed during the thermal treatment of the samples (Table 1).

The bandwidth of the E_g band is also sensitive to the crystallite size, with its full-width at half-maximum (fwhm) increasing while the crystallite size decreases.[34,35] Our results show a fwhm of 20.5 cm^{-1} for commercial TiO_2, 38.4 cm^{-1} for TiO_2 xerogel, and 41.2 cm^{-1} for $(Ti,Sn)O_2$ xerogel. The crystallite growth of both oxides with the temperature was also detected by the reduction in the E_g fwhm in heat-treated samples, as shown in Table 1.

The peak broadening in the anatase E_g band in nanocrystalline systems has been explained using the phonon confinement model.[36,37] By this model the peak broadening is due to the contribution of phonons coming from zones out of the center of the Brillouin zone, owing to their confinement in small crystallites. However, the broadening observed in our spectra is much higher than that predicted by the phonon confinement model. Parker and Siegel,[31] Lei and co-workers,[35] and Music and co-workers[28] have attributed the additional broadening in their TiO_2 sample to the high number of oxygen vacancies present in these oxides. It is well-known that for very small particles the surface-to-volume ratio is very high and a large percentage of the atoms is near the surface. At this nanometer size, the contribution of surface atoms, which are coordinative high unsaturated, becomes very significant and this effect becomes more evident as the nanoparticle becomes smaller. By this way, the excessive peak broadening observed in the Raman spectra of our samples can be attributed to the high proportion of coordinative unsaturated TiO_x species present on this samples, due to the high surface-to-volume proportion observed in the nanometric samples obtained.

Luca and co-workers[38]have reported the relation between the surface unsaturated TiO_x species and the observed absorption edge shift on the UV−vis diffuse reflectance spectra of several TiO_2 samples. They proved the existence of such unsaturated species on their sample using the X-ray absorption spectroscopy (XAS) technique. In a similar way, we used the XAS technique to verify the occurrence of these unsaturated species in our xerogel samples, to corroborate our Raman results, and to verify the effect of Sn in the chemical environment of Ti in the $(Ti,Sn)O_2$ xerogel. The approach for the interpretation of our XAS data was based on that presented by Luca and co-workers.[38]

(31) Parker, J.; Siegel, R. *J. Mater. Res.* **1990**, *5*, 1246.
(32) Gotic, M.; Ivanda, M.; Sekulic, A.; Music, S.; popovic, S. Turkovic, A.; Furic, K. *Mater. Lett.* **1996**, *28*, 225.
(33) Ma, W.; Lu, Z.; Zhang, M. *Appl. Phys. A* **1998**, *66*, 621.
(34) Bersani, D.; Antonioli, G.; Lottici, P. P.; Lopez, T. *J. Non-Cryst. Solids* **1998**, *232*, 175.
(35) Lei, Y.; Zhang, L. D.; Fan, J. C. *Chem. Phys. Lett.* **2001**, *338*, 231.
(36) Richter, H.; Wang, Z. P.; Ley, L. *Solid State Commun.* **1981**, *39*, 625.
(37) Bersani, D.; Lottici, P. P.; Ding, X. Z. *Appl. Phys. Lett.* **1998**, *72*, 73.
(38) Luca, V.; Djajanti, S.; Howe, R. F. *J. Phys. Chem. B* **1998**, *102*, 10650.

Table 2. XANES and EXAFS Data of Samples

sample	A_1 (eV)	A_2 (eV)	A_3 (eV)	B (eV)	IA_2/A_3	shell	*N*	*R* (Å)	σ^2 (Å^2)
TiO_2 anatase[a]	4968.8	4970.9	4972.1	4974.5	0.4073	1	6	1.948	
						2	4	3.039	
TiO_2 xerogel	4968.9	4971.0	4972.1	4974.6	0.8750	1	5.1	1.93	0.0028
						2	3.8	3.02	0.0096
(Ti,Sn)O_2 xerogel	4968.8	4970.8	4971.9	4974.5	0.8769	1	4.9	1.93	0.0039
						2	3.8	3.03	0.0132

[a] Commercial reference sample.

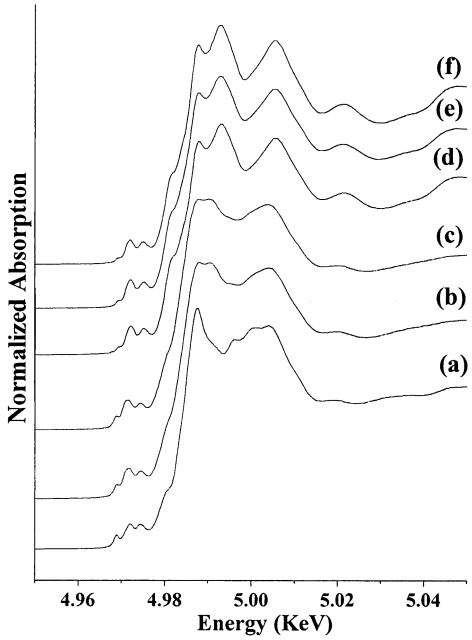

Figure 4. Normalized Ti K-edge XANES spectra of commercial anatase TiO_2 (a), TiO_2 xerogel (b), (Ti,Sn)O_2 xerogel (c), TiO_2 xerogel heat-treated at 1000 °C (d), (Ti,Sn)O_2 xerogel heat-treated at 1000 °C (e), and commercial rutile TiO_2 (f).

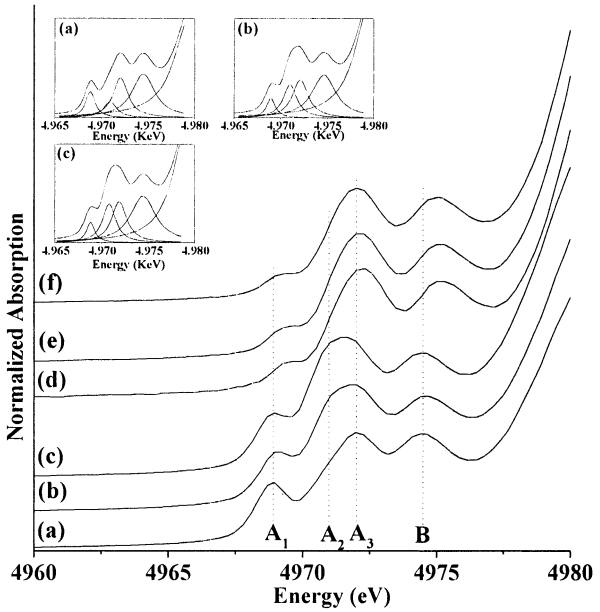

Figure 5. Normalized Ti K-edge XANES spectra in the pre-edge region (4960−4980 eV) of commercial anatase TiO_2 (a), TiO_2 xerogel (b), (Ti,Sn)O_2 xerogel (c), TiO_2 xerogel heat-treated at 1000 °C (d), (Ti,Sn)O_2 xerogel heat-treated at 1000 °C (e), and commercial rutile TiO_2 (f). Inserts show the Gaussian-fitted spectra of samples (a), (b), and (c).

Significant information about the coordination of Ti atoms in TiO_2 samples can be obtained in the pre-edge region of their XANES spectra.[38−40] This region comprehends the low-energy region between the absorption threshold and the absorption jump. The XANES spectra of the compounds synthesized in this work are shown in Figure 4, with the spectra of the commercial anatase and rutile and the spectra of the synthesized oxides heat-treated at 1000 °C. The pre-edge region of these spectra is shown in detail in Figure 5. The pre-edge structure of the Ti−K-edge for Ti atoms in octahedral sites features three peaks (named A_1, A_3, and B), and a fourth peak A_2 indicated on the low-energy side of the central A_3 peak.[38] The pre-edge spectrum is significantly different from that for Ti atoms in tetrahedral sites, where only one sharp peak is observed.[40,41] The spectra in Figure 5 show the four peaks discussed earlier, showing that Ti atoms are located in an octahedral environment in both TiO_2 and (Ti,Sn)O_2 xerogel, as expected for the anatase structure.

According to the literature, the occurrence of the A_2 peak is associated with low-coordination Ti atoms located on the surface of the crystals.[38,42] Luca and co-workers[38] observed that the ratio of the intensities of the A_2 to A_3 peaks increases as particle size decreases due to an increased contribution from the low-coordinated Ti species situated on the nanocrystals surface. We have used a similar approach to calculate the I_{A_2}/I_{A_3} ratio of our sample. The four pre-edge peaks on each spectrum were fitted, aiming to calculate the intensity and position of each peak. The results are shown in the inserts of Figure 5. The I_{A_2}/I_{A_3} values obtained were 0.4073 for commercial anatase, 0.8750 for the obtained TiO_2, and 0.8769 for (Ti,Sn)O_2. These results confirm that both TiO_2 and (Ti,Sn)O_2 xerogels are obtained in nanometric size, and the (Ti,Sn)O_2 is smaller than the TiO_2. All the XANES data are summarized in Table 2.

The postedge region of the Ti K-edge XANES (from 4.98 to 5.02 keV) contains a number of 3s → np transitions. As can be seen in Figure 4, these transitions become poorly resolved as the particle diameter decreases, in agreement with that observed by the anatase samples prepared by Luca and co-workers.[38]

The experimental EXAFS spectra were fitted (Figure 6) and Fourier-transformed (Figure 7). The FTs show clearly three peaks due to the existence of three shells of backscattering atoms around the central Ti. The first

(39) Chen, L. X.; Tijana, R.; Wang, Z.; Thurnauer, M. C. *J. Phys. Chem. B* **1997**, *101*, 10688.
(40) Wu, Z. Y.; Ouvrard, G.; Greisser, P.; Natoli, C. R. *Phys. Rev. B* **1997**, *55*, 10382.
(41) Kim W. B.; Choi, S. H.; Lee, J. S. *J. Phys. Chem. B* **2000**, *104*, 8670.
(42) Chen L. X.; Rajh T.; Jager W.; Nedeljkovic J.; Thurnauer, M. C. *J. Synchrotron Radiat.* **1999**, *6*, 445.

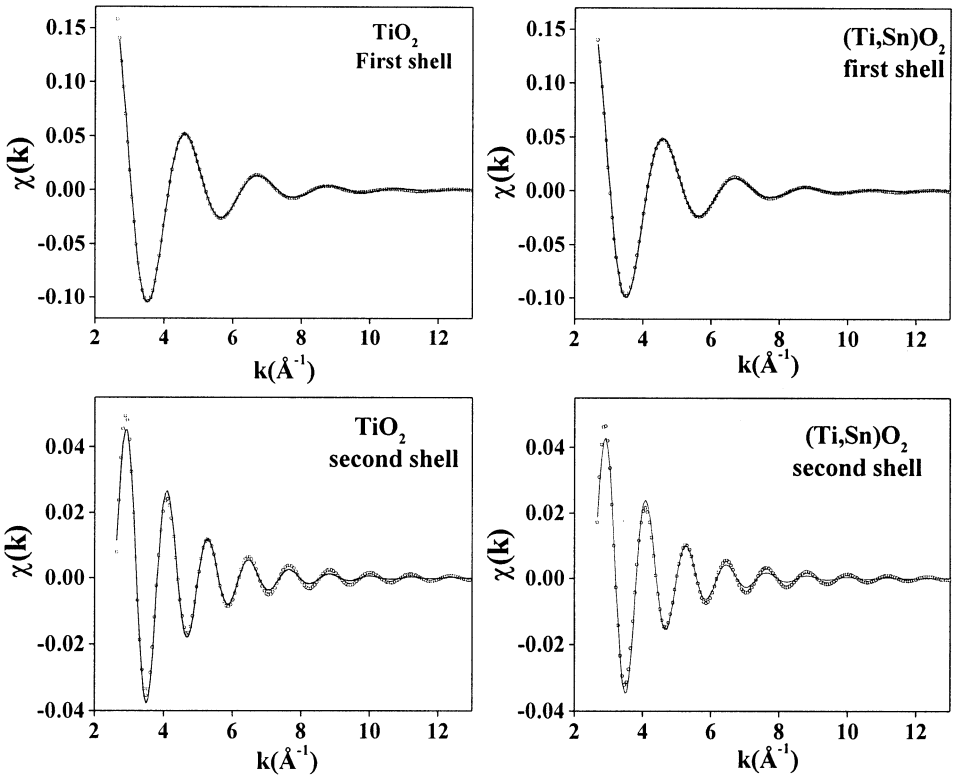

Figure 6. Experimental (dotted line) and fitted (continuous line) Ti K-edge spectra of TiO_2 and $(Ti,Sn)O_2$ xerogel samples.

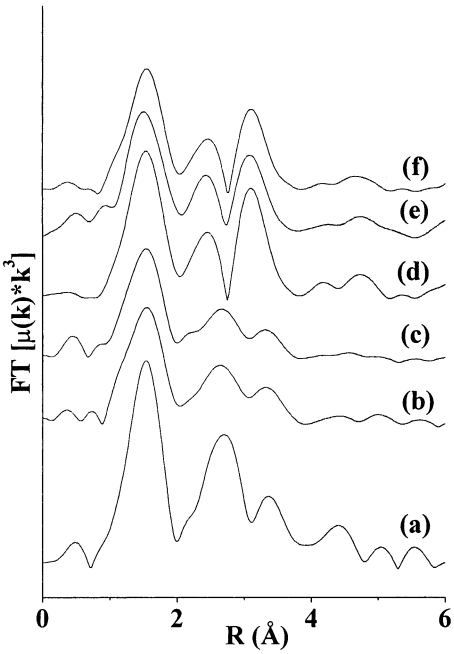

Figure 7. Normalized magnitude Ti K-edge FT-EXAFS spectra of commercial anatase TiO_2 (a), TiO_2 xerogel (b), $(Ti,Sn)O_2$ xerogel (c), commercial rutile TiO_2 (d), TiO_2 xerogel heat-treated at 1000 °C (e), and $(Ti,Sn)O_2$ xerogel heat-treated at 1000 °C (f).

and second shells are due to single Ti−O and Ti−Ti scattering paths, respectively, and the third peak is due to single and multiple scattering from a variety of paths. As can be seen in Figure 7, there is a reduction in amplitude of the FT peaks of the samples obtained in this work when compared with the bulk anatase used as reference. Also, our xerogel samples present the higher shells peaks with lower intensity relative to the first-shell peak than that observed for the reference sample. These effects have been correlated with the decrease in the particle size.[38]

The best-fit EXAFS data of the samples prepared in this work are listed in Table 2. The parameters for bulk anatase and rutile were obtained from crystallographic data. Only the first and second FT peaks were fitted for each sample due to the contributions from both single and multiple scattering paths attributed to the third peak. As can be observed, the first-shell coordination number for the Ti in the TiO_2 xerogel and $(Ti,Sn)O_2$ xerogel is lower than that observed for bulk anatase. Also, there is a more pronounced reduction in the first-shell coordination number in $(Ti,Sn)O_2$ xerogel than the TiO_2 xerogel. The average Ti−O bond length is also slightly lower than the reference anatase for both TiO_2 and $(Ti,Sn)O_2$ xerogel. Contracted Ti−O bond lengths have been observed in anatase samples with nanometric crystallite sizes, and this effect has been correlated with the reduction in the Ti coordination number due to the high surface-to-volume ratio observed in small particles.[38,39] The first-shell coordination number calculated for the samples together with the slightly contracted value of Ti−O bond length and the XANES data discussed earlier are indubitable evidence that our sol−gel samples contain titanium in lower coordination. The fact that the coordination number of Ti in $(Ti,Sn)O_2$ xerogel is lower than that observed in TiO_2 xerogel corroborate the XRD and Raman data and confirm that the presence of Sn produces mixed-oxide particles smaller than those obtained for pure TiO_2 by a similar route.

The second-shell Ti−Ti distances are very close to those of crystalline anatase. The Ti−Ti second-shell coordination number shows similar values for both TiO_2 and $(Ti,Sn)O_2$ xerogel. The small reduction in this

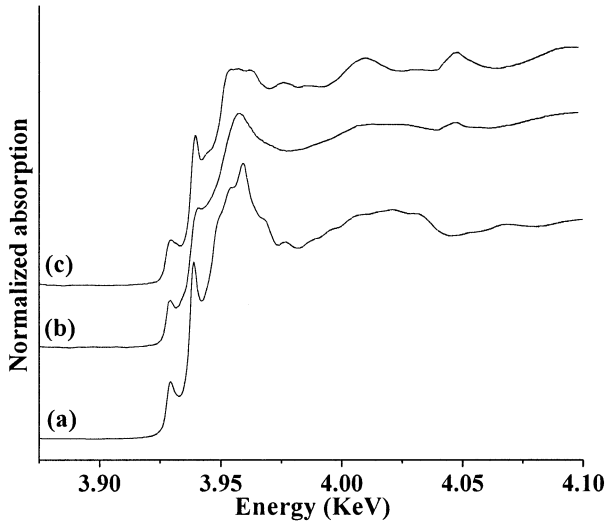

Figure 8. Normalized Sn L_3 XANES spectra of commercial SnO_2 (a), (Ti,Sn)O_2 xerogel (b), and (Ti,Sn)O_2 xerogel heat-treated at 1000 °C (c).

coordination number can be attributed to both the small size of the particles and the occurrence of a minor disorder in the lattice of the oxides nanoparticles. The increase in the Debye−Waller factor can be an evidence for this last trend (Table 2). An important piece of data present in Table 2 is a significant increase in the second-shell Debye−Waller factor of (Ti,Sn)O_2 xerogel when compared with the TiO_2 xerogel, which can indicate an increase in the disorder with the substitution of titanium by tin in the anatase lattice.

Unfortunately, we were not able to make EXAFS measurements in the Sn edge of the mixed-oxide sample. The Sn L_3 XANES spectra of the (Ti,Sn)O_2 xerogel and of this sample after heat treatment at 1000 °C are shown in Figure 8. The reference spectra of bulk cassiterite SnO_2 are included for comparison. Jiménez and co-workers[43,44] recently published the first Sn L_3 XANES spectra of nanostructured SnO_2. They applied the mathematical method of factor analysis to the XANES spectra to determine the percentage of amorphous phase in their samples. To our knowledge there is no rigorous theoretical approach aiming to identify the features observed in the Sn L_3 XANES spectra. The pre-edge region of all the spectra shown in Figure 8 are very similar, but we can note that the postedge region of the (Ti,Sn)O_2 xerogel sample shows less defined shapes, as observed also in the spectra of nanostructured SnO_2 published by Jiménez and co-workers.[43,44] As well as that observed in the Ti K-edge XANES spectra, this effect can be associated with the small particle diameters of the samples.

Conclusions

We presented here an effective sol−gel route to tin−titanium mixed oxide with anatase structure. The combination of thermal analysis, XRD, Raman, XANES, and EXAFS measurements confirms that the mixed oxide was formed as a solid solution. The presence of Ti with reduced coordination number was observed by XANES and EXAFS, and these species can be related to the excessive peak broadening observed in the Raman spectra of both TiO_2 and (Ti,Sn)O_2 xerogel spectra.

One interesting effect observed in this work is that the particle size of the mixed oxide was smaller than that observed for the TiO_2 obtained in a similar way, which can signify that the presence of tin precursor in the reactional media might be used to control the particle size of the oxides. Recently, Leite and co-workers[45] reported a novel approach to control particle size of SnO_2 prepared by the polymeric precursor method, using Nb_2O_5 as dopant. They observed that the 5 mol % Nb_2O_5 doped SnO_2 is formed with lower crystallite size than the pure SnO_2, with a SnO_2−Nb_2O_5 solid solution restricted to the surface of particles. The lower crystallite size of doped particles was attributed to this surface effect, with the Nb_2O_5 preventing the formation of necks between particles and the process of coalescence. This way, a similar effect can be occurring in our tin−titanium mixed-oxide samples, which could explain the smaller size of our mixed-oxide particles. The differences observed between the DSC profile of TiO_2 and (Ti,Sn)O_2 xerogels (Figure 1) can be evidence that the TiO_2−SnO_2 solid solution occurs in the surface of the former oxide (once the DSC events in this region show differences in the surface-adsorbed water and alcohol displacement). Other experimental results related to adsorption of Lewis bases on the surface of these xerogels also point in this direction.[46] Work is actually in progress to prove this hypothesis. Photocatalytic measurements using the mixed oxide are also under current investigation.

Acknowledgment. Research was partially performed at LNLS−National Synchrotron Light Laboratory, Brazil (Project XAS 902/01 and XAS 1030/01). Authors thank Laboratório de Espectroscopia Molecular-IQ-USP-SP, for the Raman spectra, LACTEC for the X-ray diffractograms, Dr. N. Watanabe for the XAS discussions, Dr. J. D. Motta Neto for the English revision, and CNPq, Fundação Araucária and Rede de Materiais Nanoestruturados (MCT/FINEP) for financial support. M.M.O. thanks also CAPES for the fellowship.

CM0210344

(43) Jimenez, V. M.; Caballero, A.; Fernandez, A.; Espinós, J. P.; Ocaña, M.; González-Elipe, A. R. *Solid State Ionics* **1999**, *116*, 117.
(44) Jimenez, V. M.; Espinós, J. P.; Caballero, A.; Contreras, L.; Fernandez, A.; Justo, A.; González-Elipe, A. R. *Thin Solid Films* **1999**, *353*, 113.
(45) Leite, E. R.; Weber, I. T.; Longo, E.; Varela, J. A. *Adv. Mater.* **2000**, *12*, 965.
(46) Schnitzler, D. C.; Zarbin, A. J. G., to be published.